Visual Observation of Boiling in Batch-Style Water Targets

J. Peeples[a,1], M. Stokely[a], M. Poorman[a], M. Magerl[b], B. Wieland[a]

[a]BTI Targetry LLC, 1939 Evans Rd. Cary, NC, USA
[b]IBA Molecular, 801 Forestwood Dr. Romeoville, IL, USA

Introduction

Batch-style water targets are commonly used to produce F-18, via the $^{18}O(p,n)^{18}F$ reaction. These targets are known to operate under boiling conditions in the target irradiation chamber, but the distribution of vapor under steady-state conditions was previously unknown.

The maximum operational power for a target is limited by its heat rejection capabilities. Excessive voiding, due to exceeding these capabilities, can lead to beam penetration and a corresponding decrease in saturation yield. Thermal performance of batch targets has been correlated to average void in the target [1], but the simplified assumptions of such models do not represent the true non-uniform boiling behavior.

Visualization targets allow direct viewing of the irradiation chamber during target operation [2-5]. Insight into the underlying phenomena can be used to facilitate the design of new targets with improved capabilities and to improve the accuracy of modeling techniques.

Target	Fill Vol. (mL)	Pressure (psi)	Power (W)
Heselius, et. al.[2]	0.3-0.6	50	58-220
Hong, et. al.[3]	4.5	400	300-600
Hong, et. al.[5]	4.5	0-1250	750
Peeples, et. al.[4]	2.5	70-300	0-1100
This Work	2.3-4.3	100-200	0-1260
Typical Batch[6-11]	2-4	400	1000-3000

TABLE 1. Properties of prior visualization targets

Commercial BTI Targetry targets operate at 28-35 bar (400-500 psi) with heat inputs of 1 to 3 kW and fill volumes of 2 to 4 mL [6, 7]. Existing literature on prior visualization targets documents boiling behavior at disparate pressures, power levels, and fill volumes, as shown in TABLE 1. Operation has typically been limited to power levels significantly below those used in modern production targets, limiting the utility of the results. Recently, a visualization target featuring two transparent viewing windows was used to observe boiling conditions for realistic operating beam power, target pressure, and fill volume [4]. The same methodology has been applied to three additional visualization targets to examine the effect of target geometry on observed boiling phenomena.

Material and Methods

The original visualization target, shown in FIG. 1, featured an aluminum body with a 0.127 mm (0.005 in) integral aluminum beam window and two viewing windows made of optically clear sapphire (Al_2O_3). It was operated on an IBA 18/9 cyclotron with 18 MeV protons at beam power up to 1.1 kW, for pressures of 5 to 21 bar (70 to 300 psi), and a fill volume of 2.5 mL.
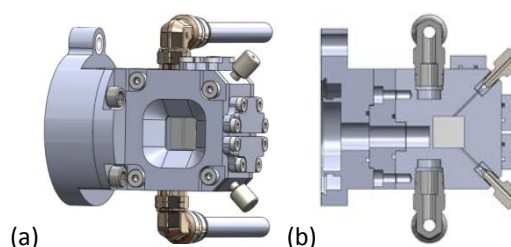

(a)   (b)

FIGURE 1. Original visualization target solid model (a) isometric view and (b) cross-section view

The three new designs all featured a wider chamber to allow for higher beam transmission and an increased chamber height, consistent with current trends in high power targets. Beam was collimated to 10 mm in the original visualization target and to 12 mm in the new designs. The chamber height was increased by fifty percent, from 15 mm to 22.5 mm.

One target featured a reduced chamber depth, and another had a ramp in the back of the chamber to reduce fill volume. Target pressure was limited to a maximum of 14 bar (200 psi) due to the larger diameter beam window. The chamber dimensions of the four visualization targets are shown in FIG. 2 and TABLE 2.
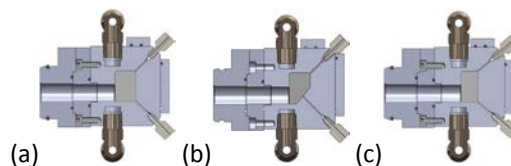

(a)   (b)   (c)

FIGURE 2. Cross-section views of (a) tall, (b) ramp, and (c) shallow visualization targets

[1]Corresponding author, E-mail: peeples@brucetech-targets.com

Target	Width (mm)	Depth (mm)	Height (mm)	Fill Volume (mL)
Original	14	15	15	2.5-3.2
Tall	16.2	15	22.5	3.1-5.5
Ramp	16.2	5-15	10.5-22.5	2.2-4.5
Shallow	16.2	12	22.5	2.5-4.4

TABLE 2. Summary of visualization targets

A video camera was used to record the boiling conditions observed for each target under several lighting conditions. From the camera view, beam enters the chamber from the left, as illustrated in FIG. 3.
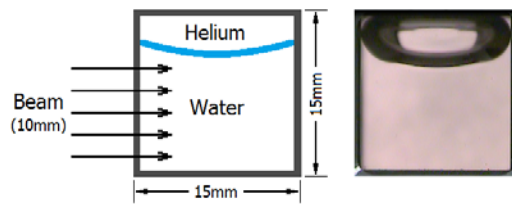

FIGURE 3. Camera view through original target

During irradiation, the proton beam excites the water molecules, producing visible blue light emissions during de-excitation. These light emissions provide a good indication of the proton range as a function of height. With good ambient lighting, the width of the Bragg peak and natural circulation effects are clearly visible. A strong backlight can be used to produce clear images of the size and distribution of bubbles generated during the boiling process. Use of no external lighting is best for observation of the proton range, including any beam penetration. These characteristics can be seen in FIG. 4.
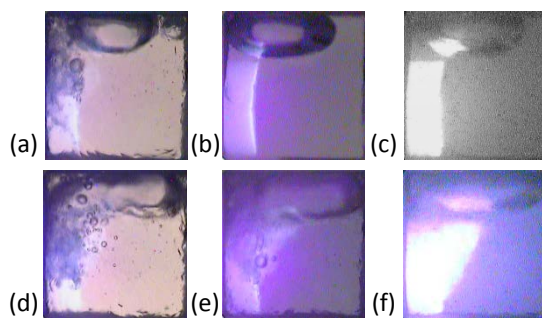

FIGURE 4. Sample images from the original visualization experiment illustrate visible features for (a) ambient and backlight, (b) ambient light, and (c) no light conditions during low power operation. Sample images for higher power operation are shown for (d) ambient and backlight, (e) ambient light, and (f) no light.

The three targets were each tested at 7 bar (100 psi) and 14 bar (200 psi) for several fill volumes. For each experimental condition, the beam current was slowly increased to determine the values corresponding to the onset of boiling and to the onset of beam penetration. Each target was tested at a fill volume of roughly 1 mm above the top of the beam strike area. If beam penetration ultimately occurred due to beam passing through the overpressure bubble, the target was tested again at a slightly higher fill volume.

The same sapphire viewing windows were used in all four visualization targets, including six days of testing in 2012 and three days of testing in 2014. After several hours of testing with the ramp target, the front sapphire viewing window cracked, as seen in FIG. 5, resulting in a loss of inventory. As a result, the shallow target was tested using an aluminum disk in place of the back viewing window. Although the backlight condition could not be achieved, natural circulation effects, boiling onset, particle range as a function of beam power and chamber height, and onset of beam penetration were still visible with a single viewing window.
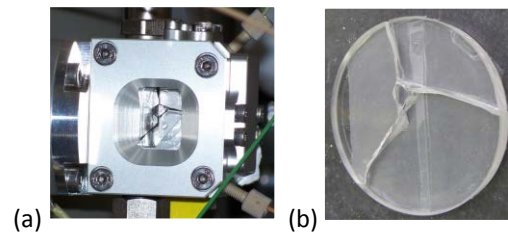

FIGURE 5. Broken sapphire viewing window (a) in ramp target and (b) removed from assembly

The cause of the break is unknown, but possible explanations include accumulated radiation damage and thermal stress. There is some evidence that the beam shifted off-center, in the direction of the broken viewing window, during operation of the ramp target. This statement is supported by asymmetric discoloration on the integral beam window and asymmetric burn marks on the back wall of the target, where beam struck the wall during the loss of inventory event. Thermal stress could be caused by the large temperature gradient on the window between the region in contact with the cool aluminum flange, at roughly 16°C (60°F), and the region in contact with the boiling water, at saturation temperature of roughly 195°C (383°F).

Results and Conclusion

For all of the visualization targets, a stable natural convection current was visible at all power levels, even before the onset of boiling. Because

[1]Corresponding author, E-mail: peeples@brucetech-targets.com

beam enters from the left side at the bottom of the target, the natural convection current is in a clockwise direction. This phenomenon is best visualized using ambient room lighting only.

For higher beam currents, bubbles form in the Bragg peak region, initiating near the center of the beam. Additional bubble formation occurs near the surface of the beam window. Bubbles formed in these regions rapidly travel upwards due to buoyancy forces. For this reason, the average void fraction in the target increases with height. The increase in void fraction leads to a reduction in density and a corresponding increase in the proton range. This behavior is exaggerated at higher beam currents, as seen in FIG. 4(f) and FIG. 7.

With the original visualization target, infrequent distribution of the helium overpressure bubble was observed at higher power levels [4]. During a disruption event, the helium bubble would descend, collapse, disperse through the chamber, and then rapidly re-collect in the top of the chamber. This behavior was not observed in the new targets, most likely due to the increased chamber height.

Two thermal limits were observed which result in some beam penetration in the top region of the beam. For lower fill volumes, steam accumulation in the helium overpressure bubble causes the bubble to expand into the beam region. The lower density of the bubble is insufficient to stop the beam, as shown in FIG. 6. For higher fill volumes, proton interactions in the water lead to boiling, and excessive voiding occurs when bubbles produced in the beam region cannot rise quickly enough out of the path of the beam, as shown in FIG. 7. The second condition corresponds to a higher total beam power. The averaged power density for each of the three visualization targets at the observed thermal limit was the same, within measurement error. At 14 bar (200 psi), the thermal limits were observed at roughly 300 W/mL, and at 7 bar (100 psi), the thermal limits were observed at roughly 270 W/mL.

For the new visualization targets, the increased chamber height was beneficial for vapor accumulation and for maintaining a stable internal pressure. Adding additional chamber depth was shown to accommodate more voiding and higher maximum operating beam power, but did not improve the averaged power density. These experiments demonstrated that a small increase in the target fill volume can potentially increase the target thermal limit, by preventing beam penetration through the overpressure bubble.
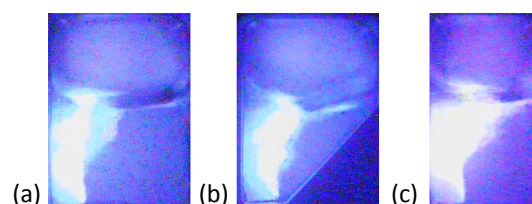

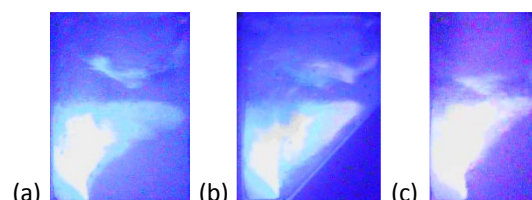FIGURE 6. Beam penetration through the overpressure bubble for (a) tall, (b) ramp, and (c) shallow targets

FIGURE 7. Beam penetration through top of bulk fluid for (a) tall, (b) ramp, and (c) shallow targets

References

1. J. L. Peeples, M. H. Stokely and J. M. Doster: *Appl. Radiat. Isot.* **69**, pp. 1349-1354, 2011.
2. S. Heselius, D. J. Schlyer and A. P. Wolf: *Appl. Radiat. Isot.* **40**(8), pp. 663-669, 1989.
3. B. H. Hong, T. G. Yang, I. S. Jung, Y. S. Park and H. H. Cho: *Nucl. Inst. Meth. Phys. Res. A* **655**, pp. 103-107, 2011.
4. J. L. Peeples, M. H. Stokely, M. C. Poorman, M. Magerl, B. W. Wieland: *AIP Conf. Proc.* **1509**, pp. 76-80, 2012.
5. B. H. Hong, J. Kang, I. S. Jung, H. G. Ram, Y. S. Park and H. H. Cho: *Nucl. Inst. Meth. Phys. Res. A* **728**, pp. 6-10, 2013.
6. M. H. Stokely, T. M. Stewart and B. W. Wieland: *120+ μA Single 18F- Target and Beam Port Upgrade for the RDS/Eclipse.* In: Proceedings of the 13th International Workshop on Targetry and Target Chemistry, 056, 2010.
7. M. H. Stokely, J. L. Peeples, M. C. Poorman, M. Magerl, T. Siemer, P. Brisard and B. W. Wieland: *AIP Conf. Proc.* **1509**, pp. 71-75, 2012.
8. J. M. Link, S. C. Shoner and K. A. Krohn: *AIP Conf. Proc.* **1509**, pp. 61-65, 2012.
9. S. Eberl, T. Eriksson, O. Svedberg, J. Norling, D. Henderson, P. Lam, T. Bourdier and M. Fulham: *AIP Conf. Proc.* **1509**, pp. 66-70, 2012.
10. W. Gelbart, R. R. Johnson, B. Abeysekera, L. Matei and D. Niculae: *All-Metal Water Target with Spherical Window.* In: Book of Abstracts for WTTC15, pp. 113-114, 2014.
11. F. Devillet, J. M. Geets, M. Ghyoot, E. Kral, R. Mooij, B. Nactergal and M. Vosjan: *High power conical-shaped Niobium targets for reliable [^{18}F$^-$] production and lower [^{18}O] water consumption.* In: Book of Abstracts for WTTC15, pp. 117, 2014.

[1]Corresponding author, E-mail: peeples@brucetech-targets.com